Computational and Theoretical Chemistry 1059 (2015) 27–34

Contents lists available at ScienceDirect

Computational and Theoretical Chemistry

journal homepage: www.elsevier.com/locate/comptc

Interaction of aluminum dimer with defective graphene

Nicolás F. Domancich [a], Ricardo M. Ferullo [b], Norberto J. Castellani [a,*]

[a] Grupo de Materiales y Sistemas Catalíticos, Instituto de Física del Sur, Departamento de Física, Universidad Nacional del Sur, Av. Alem 1253, 8000 Bahía Blanca, Argentina
[b] Instituto de Química del Sur, Departamento de Química, Universidad Nacional del Sur, Av. Alem 1253, 8000 Bahía Blanca, Argentina

ARTICLE INFO

Article history:
Received 30 September 2014
Received in revised form 22 January 2015
Accepted 6 February 2015
Available online 26 February 2015

Keywords:
Graphene monovacancy
Aluminum dimer
Adsorption
DFT

ABSTRACT

In the present work, density functional theory (DFT) calculations using cluster and slab models were performed in order to study the adsorption of Al dimer on a monovacancy of graphene. With cluster models, two different approaches were considered for the exchange and correlation functional; namely, the Perdew, Burke and Ernzerhof (PBE) and the Becke, 3-parameter, Lee–Yang–Parr (B3LYP) functionals. Under the slab approximation only PBE was employed. The geometry where two Al atoms are simultaneously adsorbed on both sides of a monovacancy (H3–H3) is the most stable thermodynamically, followed by the structure in which one Al atom resides over the center of a vacancy and the other makes a bridge between two carbon atoms (H3-B). The magnitude of the Al_2 adsorption energy is larger than that of an adsorbed Al atom. While the ground states for both free Al_2 and isolated defective graphene is predicted to be a triplet, that corresponding to the dimer adsorbed on the monovacancy is calculated to be a singlet. Charge population analysis has shown that a significant electron transfer from Al to the substrate of about 2*e* is produced. The corresponding density of states (DOS) obtained with periodic conditions indicate that the Al_2/defective graphene system at the H3-B geometry with a doping level of about 3% has a nearly zero band gap with almost no states at the Fermi level, unlike the situation where only one Al atom is adsorbed on the monovacancy which present a metal-like behavior.

1. Introduction

Graphene is a bidimensional material with remarkable electronic transport properties and unusual thermal, optical and mechanical characteristics. The very high specific surface of graphene makes this material as an ideal support for catalysts and gas sensors [1]. The challenge of adapting its intrinsic properties related to electronic conductivity by means of the adsorption or insertion of foreign atoms is a widely studied issue both experimentally as theoretically [2].

The presence of defects on the graphene surface modifies its adsorptive properties since it produces non-equivalent carbon atoms that show higher reactivity for adsorption. Monovacancies and multivacancies are considered as typical defects of reduced graphene oxide sheets or ion-sputtered graphene [3]. Photoelectron spectroscopy results for Al deposited on highly oriented pyrolitic graphite that exposes regular graphene sheets indicate that no chemical reaction occurs at any temperature. Conversely, studies of Al deposition on ion-sputtered samples give evidence that Al–C bonds appear with charge transfer from Al to C [4].

The adsorption of Al atoms on regular and defective graphene with monovacancies has been considered theoretically [5] within the density functional theory (DFT) formalism. These studies reveal a chemical bond less strong than that of transition metals, accompanied with an electron transfer form Al to graphene. On the other hand, and also in the framework of DFT, the bond formed on a graphene monovacany results to be much stronger than that on any regular site [6]. The deposition of Al_n ($n = 5, 6, 13$) clusters on perfect graphite was theoretically studied by using the Car–Parrinello approach, showing a weak adsorbate–substrate interaction [7]. Recently, the adsorption of a icosahedric Al_{13} cluster with a monovacancy was studied with DFT, considering different stable geometries and the corresponding electronic structure [8]. The results are compatible with an electronic transfer from Al to C.

Another aspect of special interest is the formation of magnetic structures on a surface through the generation of defects such as monovacancies and multivacancies, the doping with foreign atoms, and the adsorption of atoms or molecules. The creation of a carbon monovacancy on graphene is accompanied with the association of dangling bonds and the appearance of local magnetism [9]. On the other hand, the atoms of elements like C and N, partially preserve their spin as adsorbed species on graphene [10], whereas the atoms of other elements as Ca, acquire spin polarization [5]. The

* Corresponding author. Tel.: +54 2914595141.
E-mail address: castella@criba.edu.ar (N.J. Castellani).

http://dx.doi.org/10.1016/j.comptc.2015.02.006
2210-271X/

insertion of B, N and P atoms is accompanied with the presence of local magnetism [10,11]. Recently, it was theoretically demonstrated that the Be_2 molecule acquires spin polarization when it is adsorbed perpendicularly on graphene [12]. Previous DFT calculations [6] have shown that when one Al atom is adsorbed on a regular graphene, electronic charge is transferred to the surface with a large delocalization of the unpaired spin. When an Al atom is adsorbed on a C monovacancy, i.e., behaving as substitutional atom, one spin of the vacancy becomes paired with the spin of the Al atom, leaving the remaining one distributed over the surface.

For dimers of one valence electron metals like Li_2 or Au_2, where the bonding arises from sigma-type interactions between half-filled atomic s orbitals, it is expected that the ground state will be $^1\Sigma_g$. On the other hand, for dimers of metals with a lone p-electron like Al_2, the chemical bond comes from the competition between σ_g or π_u bonding orbitals, giving states with $^1\Sigma_g$, $^3\Sigma_g$, $^1\Pi_u$, $^3\Pi_u$ or $^1\Delta_g$ symmetries [13], and the question is open regarding which of them will participate in the interaction with defective graphene and what spin polarization results.

In the present work the adsorption of Al_2 on a graphene monovacancy is studied, putting emphasis on the electronic structure changes undergone by the molecule and the graphene itself. The study of this system is of interest also by the role played by Al as anchoring centers for molecules in gas sensors and catalysts. With this purpose, two complementary models, clusters and slabs, have been applied both within the DFT formalism with its corresponding analysis of the electronic structure. Gaussian-03 (G03) and Vienna *ab initio* simulation package (VASP) calculation packages were used. One of the most relevant advantages in using cluster models under G03 is that it allows us to use the B3LYP hybrid functional, one of the most widely used approximation owing to its good performance, generally not implemented in plane-wave-based periodic programs.

2. Theoretical method

The present calculations are based on DFT and were carried out mainly applying a cluster model with a localized Gaussian basis set. This approach was accomplished appealing to the Gaussian-03 package [14]. To study the adsorption of Al_2 on a carbon vacancy of graphene, four central C_6 units surrounded by one crown of C_6 units saturated with H atoms was used. The resulting structure can be ascribed to that of the circumpyrene molecule without its central C atom ($C_{41}H_{16}$, see Fig. 1). Clusters of similar size have been used in the past to represent the surface of graphene [15–20]. Calculations for the cluster model were performed applying the PBE exchange and correlation functional due to Perdew, Burke and Ernzerhof [21] and the B3LYP hybrid functional [22], both at the unrestricted spin level. The adsorption energy, E_{ads}, was computed according to:

$$E_{ads} = E_{Al2/substrate} - E_{Al2} - E_{substrate} \quad (1)$$

where $E_{Al2/substrate}$, E_{Al2} and $E_{substrate}$ correspond to the Al_2/substrate, free Al_2 dimer and isolated substrate total energies, respectively. In this way, a negative value of E_{ads} corresponds to an exothermic process. The coordinates corresponding to Al atoms and their nearest C atoms were optimized looking for the E_{ads} minimum. In all the calculations the 6-31++G** basis set was used. Atomic net charges (Q) were calculated by means of the natural bond orbital (NBO) analysis [23].

Complementary calculations were performed considering a slab model. This approach to the Al_2/graphene system was accomplished appealing to the Vienna *ab initio* simulation package [24,25]. It solves the Kohn–Sham equation of DFT using a plane wave basis set. A good convergence was achieved with cut-off energy of 700 eV for the kinetic energy. The projector augmented wave (PAW) method was used to describe the effect of the core electrons on the valence states [26,27]. The exchange and correlation effects were calculated by the PBE functional. The two dimensional Brillouin integrations were performed on a grid of $5 \times 5 \times 1$ Monkhorst–Pack special k-points [28]. In order to calculate the electronic density of states (DOS) a grid of $11 \times 11 \times 1$ k-points was used. All the calculations were performed at the spin-polarized level. Defective graphene was represented by means of a 4×4 supercell with 31 carbon atoms and a gap of 20 Å in the normal direction to the sheet of graphene. This vacuum gap is large enough to avoid interaction between the adsorbed Al atoms and the periodic images of the slab. All the atoms within the supercell were allowed to relax until the residual Hellmann–Feynman forces were lower than 0.01 eV/Å. A large box of $20 \times 20 \times 20$ Å^3 was used to obtain the free Al_2 molecule energy.

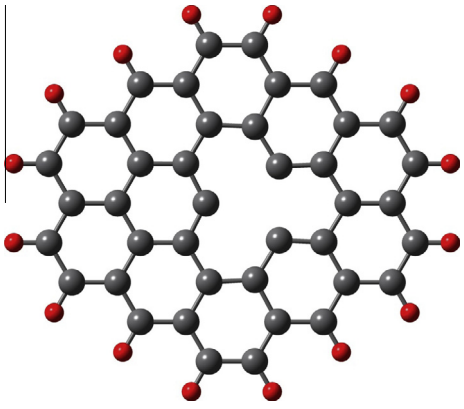

Fig. 1. $C_{41}H_{16}$ cluster model for a carbon monovacancy in graphene. C atoms: gray balls; H atoms: red balls. (For interpretation of the references to color in this figure legend, the reader is referred to the web version of this article.)

3. Results and discussion

3.1. Study of free Al_2 and isolated defective graphene

The main molecular parameters of free Al_2 molecule obtained with G03 are summarized in Table 1. The ground state obtained

Table 1
Molecular properties for different states of Al_2. G03 results.

	Symmetry	E_{dis} (eV)	d_{Al-Al} (Å)
B3LYP	$^3\Pi_u$	−1.31	2.76
		−1.40[a]	2.72[a]
		−1.41[b]	2.71[b]
		−1.34[c]	2.70[c]
	$^3\Sigma_g$	−1.18	2.51
		−1.37[a]	2.48[a]
		−1.36[b]	2.48[b]
			2.47[c]
	$^1\Sigma_g$	−0.94	3.05
	$^1\Pi_u$	−0.57	2.56
PBE	$^3\Pi_u$	−1.60	2.76
	$^3\Sigma_g$	−1.62	2.50
	$^1\Sigma_g$	−1.08	3.07
	$^1\Pi_u$	−0.91	2.54

[a] Theoretical result with correlation consistent basis sets at the internally contracted multireference configuration interaction (CMRCI) level [31].
[b] Theoretical result at coupled cluster singles and doubles with perturbative triples corrections (CCSD(T)) level [32].
[c] Experimental result from resonant two-photon ionization spectroscopy [13].

Table 2
Energies (in eV) for monoelectonic states of Al_2 and the cluster model of graphene with a monovacancy. The symmetries are indicated between brackets and the spin projection between square brackets. In the case of the cluster the parity of the wavefunctions with respect to a plane bisecting the vacancy is indicated: (+) and (−) for even or odd, respectively.

Occupancy	$^3\Pi_u$	$^1\Sigma_g$	^{3}G (V)	^{1}G(V)
Unoccupied	−1.543 (π_u) [β]	−2.610 (π_u)	−2.266 (−) [α]	−3.233 (+)
Unoccupied	−2.952 (π_u) [α]	−2.610 (π_u)	−2.400 (+) [β]	−3.263 (−)
Occupied	−4.190 (π_u) [α]	−3.630 (σ_g)	−4.554 (+) [α]	−4.302 (+)
Occupied	−4.440 (σ_g) [α]	−7.389 (σ_u)	−5.142 (+) [α]	−5.582 (−)

resulted to be a triplet, using both PBE and B3LYP. The results for singlet were also included as reference. The stability order of the low-lying states of Al_2 was object of several previous theoretical approaches. In an earlier work performed by Upton [29] at the configuration interaction (CI) level, the $^3\Sigma_g$ ground state was found. Nevertheless, further calculations [30–32] carried out with large basis sets and extended correlation effect treatments favor the $^3\Pi_u$ ground state, with the $^3\Sigma_g$ state very close in energy, between 0.02 and 0.05 eV. In our calculations, while the $^3\Pi_u$ symmetry is favored by 0.13 eV with B3LYP, compared to the $^3\Sigma_g$ one, the $^3\Sigma_g$ symmetry is slightly favored with PBE. On the other hand, the results obtained with VASP, not shown, are in agreement with those computed with G03, favoring the triplet state.

Notice that both the Al–Al distance and dissociation energy values for the $^3\Sigma_g$ symmetry obtained with B3LYP are in very good agreement with earlier experimental results and theoretical calculations [13,31,32]. While the dissociation energies obtained with PBE are 0.1–0.4 eV larger in magnitude than those with B3LYP, the geometries are very similar. The Al–Al distance is longer for $^3\Pi_u$ than for $^1\Pi_u$, while the opposite behavior is observed for the Σ symmetry.

The Al_2 electronic configuration of lowest energy obtained with B3LYP, only considering the valence 3s and 3p electrons, is $\sigma_g^2\sigma_u^2\sigma_g^1\pi_u^1\pi_u^0\pi_u^0$ for the $^3\Pi_u$ symmetry, and $\sigma_g^2\sigma_u^2\sigma_g^2\pi_u^0\pi_u^0$ for the $^1\Sigma_g$ symmetry. The energy values for the monoelectronic states corresponding to these symmetries are summarized in Table 2.

When one C atom is eliminated from the circumpyrene molecule ($C_{41}H_{16}$ model cluster), a magnetic state is produced, with the spins localized around the vacancy [3]. Our calculations performed with B3LYP and PBE by means of cluster models confirm this result because the triplet state is more favorable than the singlet by approximately 0.5 eV. The formation of this defect is accompanied by the rupture of the trigonal symmetry of the non relaxed defect, as it is shown in Ref. [6]. The monoelectronic states can be classified according to the even (+) or odd (−) eigenvalue for the reflection operation with respect to the bisector plane crossing the cluster and cutting perpendicularly the shortest C–C distance next to the vacancy. The corresponding energy values are summarized in Table 2.

3.2. Study of the Al_2/graphene system using cluster models

When cluster models were used to study the Al_2 adsorption on graphene we could identify five different geometries, designated according to the site symmetry where each Al atom adsorbs. In Figs. 2–6 the views for the final geometrical configuration adopted by the aluminum dimer are schematized. They correspond to: hollow fivefold-hollow fivefold, H5–H5, with the Al atoms residing over two nearby hollow sites; hollow threefold, H3, with only one Al atom linked and residing on the vacancy center; hollow threefold-hollow sixfold, H3–H6, where the second Al atom is near a hollow site of a graphene ring; hollow threefold-top, H3-T, with the second Al atom on-top of a C atom; and hollow threefold-bridge, H3-B, with the second atom making a bridge between two C atoms. Considering the results at B3LYP level, the five just mentioned geometrical configurations for the adsorption equilibrium have been obtained; nevertheless, the H3 geometry was not observed with PBE.

In Table 3 the results corresponding to adsorption energies and main interatomic distances are summarized, and in Table 4 the NBO net atomic charges for Al atoms and their first near C neighbors are reported. The ground states resulted to be singlets for all the geometries with the only exception of H5–H5 which is a triplet.

First we discuss the results obtained using the B3LYP functional. The different adsorption geometries can be classified in the following way, considering three categories: H5–H5, where the two Al atoms are arranged parallel to the surface; H3, where Al_2 adopts a geometry nearly perpendicular to graphene; and H3–H6, H3-T and H3-B, where one Al atom is located near the surface while the second one is farther apart.

In the first situation, H5–H5, the Al_2 molecule preserves its individuality, showing an Al–Al distance similar to that of free molecule (see Table 3). The Al–C distances are similar than those for an Al atom adsorbed on a regular hollow, ca. 2.5 Å, and the adsorption energy is nearly 2 eV smaller in magnitude than that of an Al atom adsorbed on the monovacancy [6]. On other hand, for the dimer adsorbed on H3 site, the values of adsorption energy and the Al–C distance corresponding to the nearest Al atom to the surface are close to those for an adsorbed individual Al atom on a vacancy [6]: −4.87 eV vs. −4.46 eV, and 1.89 Å and 1.84 Å, respectively.

In H3–H6, H3-T and H3-B geometries, one Al atom is located at a distance from the surface similar to that of an Al atom adsorbed on the vacancy, ca. 1.85 Å, whereas the other atom is located at a distance similar to that of an Al atom adsorbed on any of the three regular sites of graphene, ca. 2.5 Å [6]. The adsorption energy for these geometries is 0.2–0.4 eV larger in magnitude than that for Al_2 on the nearly perpendicular H3 geometry, indicating that this larger interaction is related with the formation of additional Al–C bonds in which other surface C atoms participate. Notice that for the H3–H6 geometry the Al–Al bond is weaker than in other cases, as it can be established by comparing its distance with those of H3-T and H3-B geometries, 3.37 Å vs. 2.74 Å and 2.75 Å, respectively, the latter being close to the value for free Al atom. The increase of energy suffered by the Al_2 dimer when it is constrained to the same Al–Al distance as on the adsorbed H3–H6 geometry is about 0.32 eV.

It is interesting to perform a comparison with the results of Ref. [8], where an Al_{13} nanoparticle with icosahedral symmetry is adsorbed on the monovacancy. Of the five modes found by the authors, the most stable one corresponds to the adsorption through only one Al atom anchored at the center of the vacancy. In the second stable geometry, Al_{13} links by means of two Al atoms oriented in such a way that both Al atoms are located similarly than in the H5–H5 mode. This latter adsorption is 2.36 eV less stable than when it is adsorbed by means of one Al atom. Interestingly, all our "H3" configurations are 2.3/2.7 eV more stable than that of H5–H5.

Regarding the results obtained using the PBE functional, for H5–H5, H3–H6, H3-T and H3-B geometries we can make the same observations just commented for B3LYP. The magnitude of E_{ads} is somewhat larger, by ca. 0.5–07 eV, and the interatomic distances somewhat shorter, by ca. 0.05 Å, than those corresponding to B3LYP. If we take as initial geometry for Al_2 that obtained for H3 with B3LYP, the molecule changes and adopts the more stable H3-B structure. That means that while B3LYP predicts an energetic barrier on the PES surface, connecting H3 and H3-B geometries, PBE results do not show this behavior. The mentioned B3LYP results thus suggest the existence of a metastable state for H3.

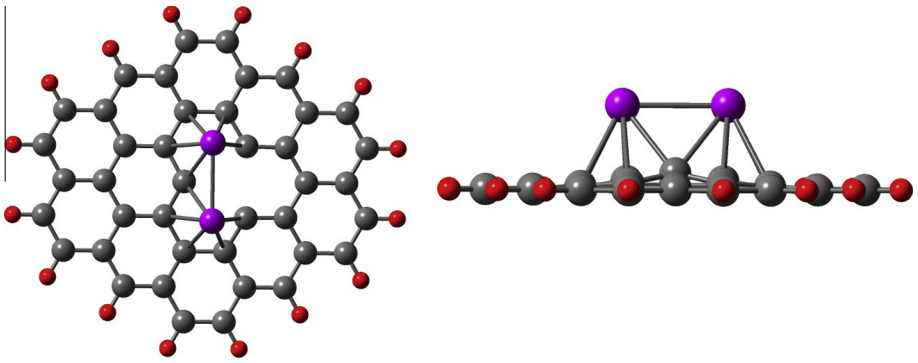

Fig. 2. H5–H5 geometry (cluster model). Left panel: top view. Right panel: lateral view. C atoms: gray balls; Al atoms: purple balls; H atoms: red balls. (For interpretation of the references to color in this figure legend, the reader is referred to the web version of this article.)

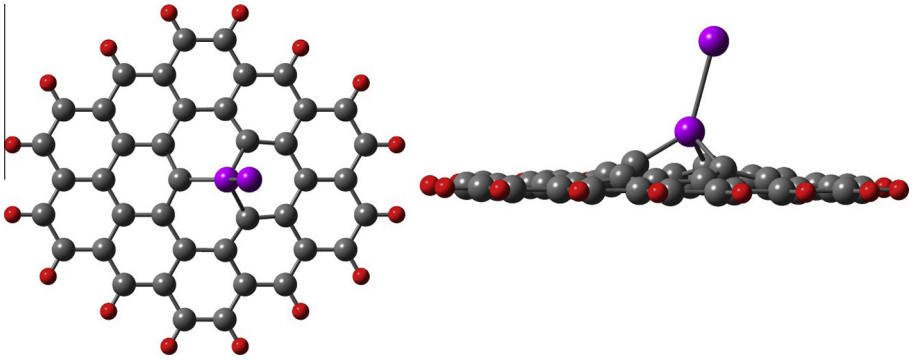

Fig. 3. As in Fig. 2 for the H3 geometry (cluster model).

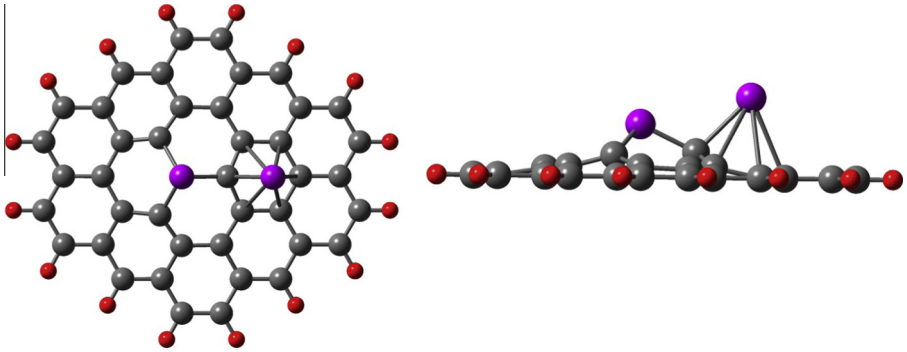

Fig. 4. As in Fig. 2 for the H3–H6 geometry (cluster model).

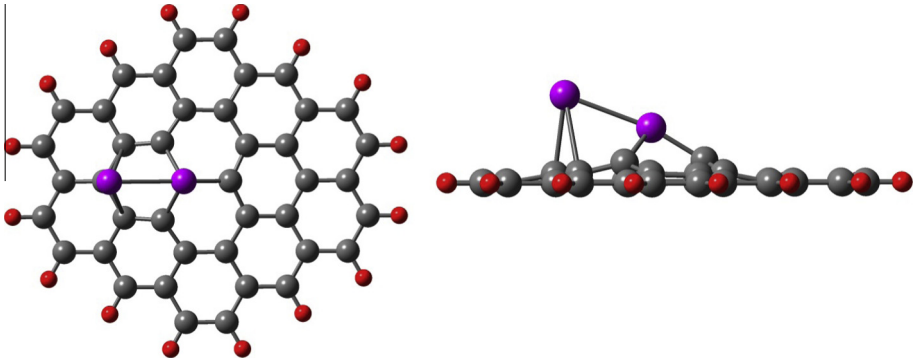

Fig. 5. As in Fig. 2 for the H3-T geometry (cluster model).

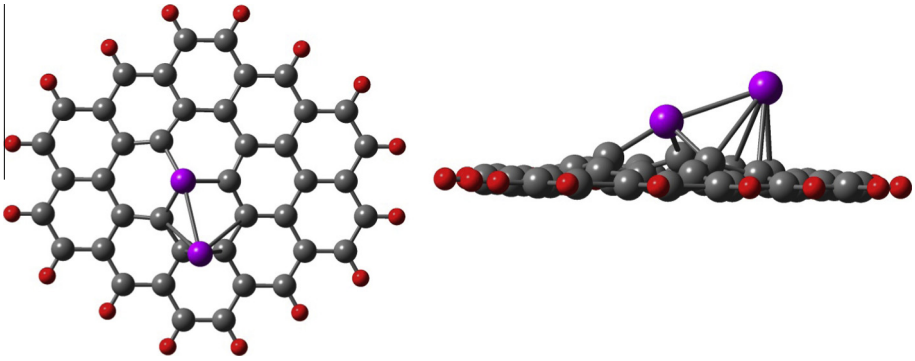

Fig. 6. As in Fig. 2 for the H3-B geometry (cluster model).

Table 3
Adsorption and dimer formation energies (in eV) and distances (in Å) for Al_2 on defective graphene.

	Geometry	E_{ads}[a]	E_{dim}[b]	d_{Al-C}	$d_{Al'-C'}$[c]	$d_{Al-Al'}$[c]
Cluster B3LYP	H5–H5	−2.54	0.78	2.468	2.468	2.745
	H3	−4.87	−1.55	1.892	3.972	2.747
	H3–H6	−5.11	−1.79	1.839	2.657	3.374
	H3-T	−5.18	−1.86	1.867	2.365	2.743
	H3-B	−5.29	−1.97	1.866	2.406	2.750
	H3–H3	−6.31	−2.99	2.000	2.000	2.610
Cluster PBE	H5–H5	−3.24	−0.33	2.429	2.429	2.645
	H3′	−4.93	−2.02	1.902	4.097	2.722
	H3–H6	−5.40	−2.49	1.859	2.603	3.350
	H3-T	−5.59	−2.68	1.888	2.298	2.686
	H3-B	−5.69	−2.78	1.886	2.353	2.693
	H3–H3	−6.66	−3.75	2.000	2.000	2.630
Slab PBE	H3	−5.89	−2.16	1.904	4.086	2.740
	H3–H6	−6.37	−2.64	1.855	2.578	3.399
	H3-B	−6.46	−2.73	1.876	2.356	2.665
	H3–H3	−7.56	−3.83	2.000	2.000	2.570

[a] Results for Al atom on defective graphene: B3LYP (G03): E_{ads} = −4.63 eV, d_{Al-C} = 1.86 Å; PBE (G03): E_{ads} = −4.53 eV, d_{Al-C} = 1.84 Å; PBE (VASP): E_{ads} = −5.51 eV, d_{Al-C} = 1.85 Å.
[b] Results for free Al_2: B3LYP (G03): d_{Al-Al} = 2.763 Å, E_{dis} = −1.31 eV; PBE (G03): d_{Al-Al} = 2.498 Å, E_{dis} = −1.62 eV; PBE (VASP): d_{Al-Al} = 2.767 Å, E_{dis} = −1.78 eV.
[c] Al refers to the nearest aluminum atom from the graphene surface; Al′ indicates the other aluminum atom. C and C′ refer to the nearest C atoms to Al and Al′ atoms, respectively.

Notwithstanding this observation, and for the sake of comparison, a complementary calculation using PBE was performed, imposing that the farther apart Al atom can be on the normal axis passing through the monovacancy center. With this constraint a geometry labeled as H3′ was obtained that follows the trend above commented for H3.

Table 4
Net NBO atomic charges, in *e* (cluster model).

	Geometry	Q(Al)[a]	Q(Al′)[a]	Q(C)[a]	Q(C′)[a]
B3LYP	H5–H5	0.690	0.689	−0.168	−0.166
	H3	0.752	0.577	−0.360	−0.360
	H3–H6	1.530	0.767	−0.602	−0.044
	H3-T	1.113	0.719	−0.434	−0.192
	H3-B	1.192	0.725	−0.453	−0.152
	H3–H3	1.120	1.120	−0.810	−0.810
PBE	H5–H5	0.704	0.705	−0.158	−0.160
	H3-T	1.088	0.722	−0.421	−0.209
	H3-B	1.145	0.729	−0.441	−0.185
	H3–H3	1.116	1.116	−0.801	−0.801

[a] Al refers to the nearest aluminum atom from the graphene surface; Al′ indicates the other aluminum atom. C and C′ refer to the nearest C atoms to Al and Al′ atoms, respectively.

Recently, the simultaneous adsorption of two Al atoms on both sides of a monovacancy was theoretically evaluated with periodic conditions at the local density approximation (LDA) level [33]. A sixth geometry, similar to that described in Ref. [33], where two Al atoms are simultaneously adsorbed on both sides of a monovacancy, was also obtained here. It was designed as H3–H3 (see Fig. 7). The corresponding values of adsorption energy and geometrical parameters were included in Table 3 and the related NBO net atomic charges in Table 4. We note that this geometry is more stable than that H3-B structure by about 1 eV. The Al–Al distance is of 2.61–2.63 Å, in between the values obtained for ground and first excited states of free Al_2 dimer; furthermore, the Al–C distance (2.00 Å) is intermediate between the Al–C distances obtained for the H3-B geometry (1.9–2.4 Å). In a previous work we have shown that for an Al atom a very high barrier of around 2.7 eV is necessary to cross the sheet through the monovacancy [6] to produce an equivalent adsorption geometry on the other side of sheet; the corresponding transition state corresponds to a situation in which the Al atom resides on the graphene plane. This high barrier is in relation with the short Al–C distances present in this structure (1.68 Å) which in turn reflects the limited space within the monovacancy to allow the migration to occur. In the case of the Al dimer, a high activation barrier is expected to pass from, for instance, the H3-B geometry to the H3–H3 one, because also in this case one Al atom must cross the graphene sheet.

In order to study the reaction process that yields the Al_2 molecule, the dimer formation energy E_{dim} was calculated. This is defined as the energy demanded to link an Al atom to a previously adsorbed one on the monovacancy. That is,

$$E_{dim} = E_{Al2/substrate} - E_{Al1/substrate} - E_{Al} \quad (2)$$

where $E_{Al2/substrate}$, $E_{Al1/substrate}$ and E_{Al} correspond to the Al_2/substrate, Al_1/substrate (with the Al atom on the monovacancy) and isolated Al atom total energies, respectively. The corresponding values for E_{dim} are summarized in Table 3. We observe that this quantity is larger for the geometries with larger E_{ads}, and that the magnitude of E_{dim} obtained with PBE is 0.5–07 eV larger than those with B3LYP. Particularly, at B3LYP level, it is not possible to form the Al–Al bond for H5–H5. A remarkable result is the fact that, with the exception of the H5–H5 geometry, the magnitude of E_{dim} is always larger than that of the dissociation energy for free Al_2, showing that the graphene substrate strongly enhances the Al–Al bonding. On the other hand, as commented above, the anchoring of two Al atoms on both sides of a monovacancy was studied by calculating the binding energy of one Al atom to an Al-doped graphene surface with periodic conditions at the local density approximation (LDA) level [33], obtaining a value of −3.91 eV (with an Al–Al distance of 2.54 Å). This quantity corresponds to our definition of E_{dim}. The corresponding calculation with our cluster models gives a value of −2.99 eV at

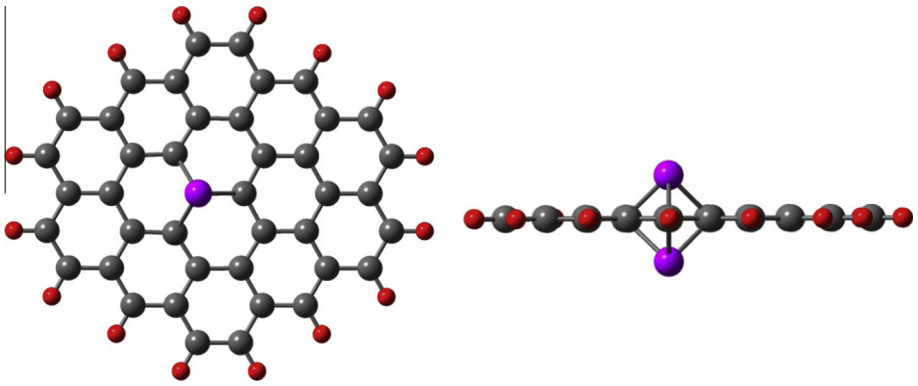

Fig. 7. As in Fig. 2 for the H3–H3 geometry (cluster model).

the B3LYP level and −3.75 eV at the PBE level (with Al–Al distances of 2.61 and 2.63 Å, respectively). We notice the satisfactory agreement between both approaches.

A relevant feature to underline is the fact that, while the lowest energy state for both free Al_2 dimer and isolated defective graphene is a triplet, when Al_2 adsorbs on the monovacancy, a singlet is obtained. The last is 0.6–0.7 eV more stable than the triplet state, a result that contrast with the energy difference favoring the triplet for the individual fragments, that is of 0.1–0.5 eV. This means that the quenching of magnetism of the graphene defect was obtained at the expense of a great stabilization of the non magnetic state.

In Fig. 8, the HOMO−1, HOMO, LUMO and LUMO+1 orbitals corresponding to the Al_2 dimer with the H3-T geometry have been schematized. This geometry is appropriate because it allows both to classify the monoelectronic states according to their parity regarding the reflection (σ_v) on the bisector plane crossing the vacancy and, at the same time, to individualize more easily the contribution of monolectronic states of Al_2 as a fragment. It can be observed that the HOMO, LUMO and LUMO+1 orbitals are of even parity, whereas the HOMO−1 orbital is odd. Moreover, comparing the signs within the Al–C region, it is evident that the HOMO–LUMO orbitals can be viewed as a bonding–antibonding pair. The HOMO has a clear bonding character, which contributes strongly to stabilize the singlet state. In principle, the HOMO and HOMO−1 orbitals of Al_2/defective-graphene would come from the combinations of the triplets of the individual fragments. Nevertheless, it is no easy to make a clear energy diagram from the monoelectronic states of Al_2 and monovacancy considering the orbital symmetries. Particularly, as above mentioned, the HOMO−1 orbital of the Al_2/graphene system has odd parity with respect to the σ_v reflection whereas all the possible bonding and antibondig combinations of frontier orbitals of Al_2 and monovacancy as separated fragments have always even parity. The spatial distribution of this orbital bears a similarity to that of the HOMO−1 orbital (not shown) of the singlet for the monovacancy, so that it results to be essentially a non-bonding MO with respect to the Al–C contact.

Looking at Table 4, we can observe that the Al atoms and their near neighbor C atoms acquire systematically net positive and negative charges, respectively. This electronic transfer from the metal atoms to graphene indicates the existence of an electrostatic interaction between these two components. This result is in agreement with previous theoretical results [8] and earlier experimental evidence [4]. For the more stable geometries the charge transfer is 1.8–2.3e. We notice also that this effect is less relevant for H5–H5 and H3 geometries, which is 1.3–1.4e. Moreover, when an isolated Al atom is adsorbed a transfer of 0.8–0.9e is obtained. From Table 2 we can see that the SOMO (highest singly occupied molecular

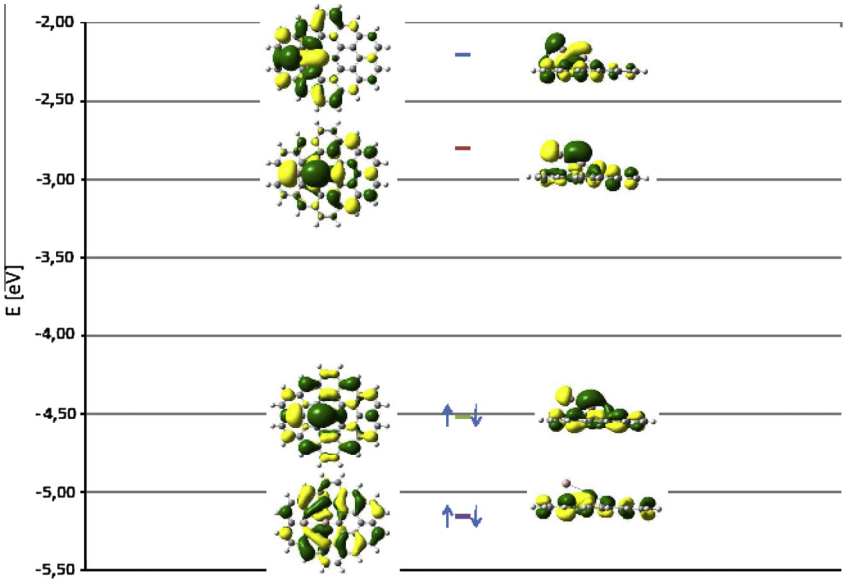

Fig. 8. Molecular orbitals of the Al_2/graphene system for the H3-T geometry. Left panel: top view. Right panel: lateral view.

orbital) and the SOMO−1 of Al_2 (triplet state) have higher energies than the SOMO and SOMO−1 of defective graphene (also at triplet state). As a consequence, an electron charge transfer occurs from Al_2 to graphene by pairing the electrons and forming the stable Al_2/graphene closed-shell structure.

To our knowledge, no theoretical calculations on Al_2/defective graphene or carbon nanotubes (CNTs) have been published previously, apart from the previous study for Al adsorbed on doped graphene above commented [33]. On the other hand, we can mention studies with other metal dimers such as Pt_2 [34], Au_2 and Fe_2 [35] on a graphene monovacancy. The most stable geometry for Pt_2 is near-parallel to the surface. The adsorption energy is similar to that of an individual Pt atom on the site, −7.26 eV vs. −7.45 eV. The more stable geometries for Au_2 and Fe_2 correspond to bended molecules, with H3–H5 and H3-quasi-T geometries, respectively. The adsorption energy is similar to that of an individual atom, −2.55 eV vs. −2.45 eV, in the case of Au_2, whereas it shows an important destabilization, −4.90 eV vs. −7.62 eV, in the case of Fe_2. In all the cases an electron transfer is produced from the metal dimer to graphene. The same tendency predicted for Fe_2 is observed here for Al_2, although less pronounced, with adsorption energies of −4.63 eV for atomic Al and −5.29 eV for Al_2 at H3-B, respectively (B3LYP calculations).

3.3. Study of the Al_2/graphene system using slab models

In Table 3 the main energetic and geometrical parameters are summarized. Notice that only the H3, H3–H6, H3-B and H3–H3 geometries were found. In particular, in the H3–H6 situation the Al–Al bond is largely weakened. As before, for all these geometries the ground state corresponds to a singlet. The E_{ads} values are 0.8–1.0 eV larger in magnitude than those calculated with the cluster approach with PBE, and preserving the same H3-B < H3–H3 ordering. The distances are at most 0.06 Å longer by using the slab model. Regarding the E_{dim} values, we notice that they are very similar, with differences in the range of 0.05–0.15 eV. Hence, there is a satisfactory comparison between both methods.

The electronic structure of Al_2/graphene was further analyzed in terms of the DOS using the same slabs, which implies a C:Al_2 relation of 31:1 (i.e., a doping level of about 3%). We have considered two situations, both with the Al dimer adsorbed on one side of the graphene sheet: H3 and H3-B. Taking into account that the most stable structure (H3–H3) is difficult to achieve from any of the other adsorbed Al_2 structures due to the above commented arguments, geometries such as H3 or H3-B are more interesting to study from this point of view. Firstly, for the sake of comparison,

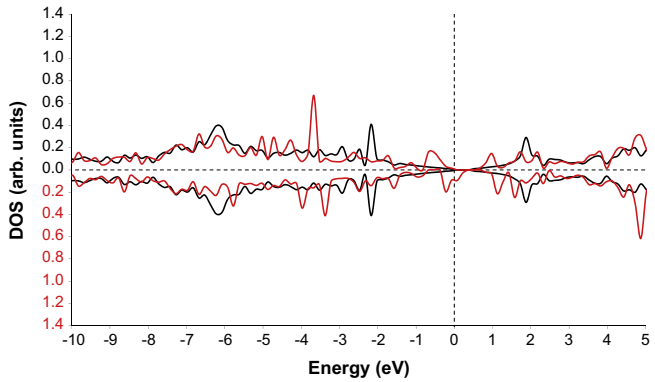

Fig. 9. DOS of regular and defective graphene. Black line: regular graphene; red line: graphene with monovacancy. The zero of energy corresponds to the Fermi level. Spin up: upper panel; spin down: lower panel. (For interpretation of the references to color in this figure legend, the reader is referred to the web version of this article.)

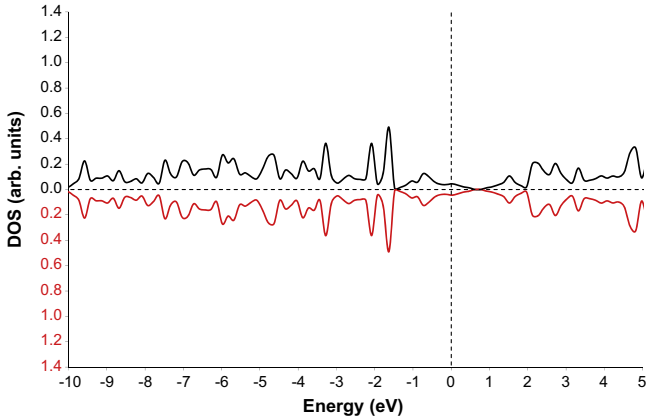

Fig. 10. DOS of Al atom on defective graphene. The zero of energy corresponds to the Fermi level. Spin up: upper panel; spin down: lower panel.

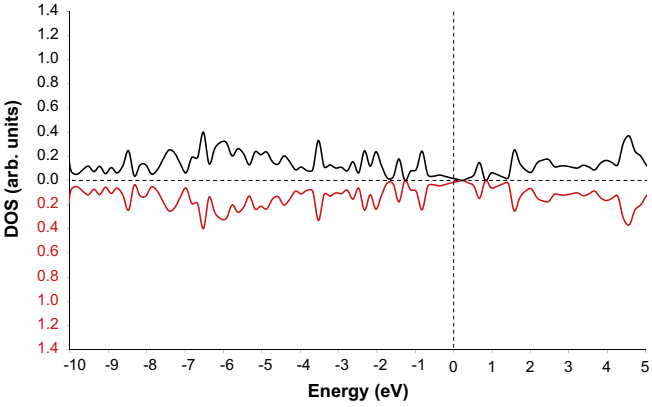

Fig. 11. As in Fig. 10 for Al_2/graphene; H3-B geometry.

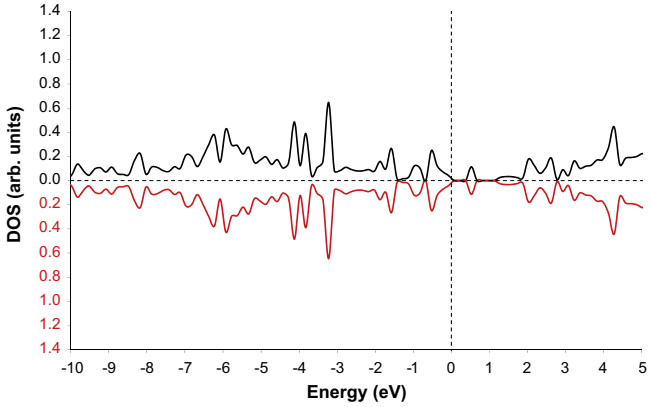

Fig. 12. As in Fig. 10 for Al_2/graphene; H3 geometry.

in Fig. 9 the DOS of regular and defective graphene are represented in the same graphic. We observe the zero band gap character for the regular surface with no states at the Fermi level and, conversely, the appearance of specific states at the Fermi level for the defective surface. In addition, an unbalance is produced between the integrated DOS profile for up and down spin projections, giving a magnetic moment of 0.60 μ_B per cell [15], in correspondence with the presence of magnetism in the monovacancy. We want to underline that for infinite single-vacancy defective graphene, the ground state is not triplet as in the case of the cluster

model in Section 3.1, because in DFT-periodic methods as the one implemented in VASP it is possible to perform calculations without fixing the value of the magnetic moment. When an Al atom is adsorbed on this defect, the unbalance disappears, giving a metallic non-magnetic system (Fig. 10). The insertion of a second Al atom modifies the electronic structure, as it is shown in Figs. 11 and 12 for H3-B and H3, respectively. In the latter cases, a nearly zero band gap appears, similarly to the case of regular graphene. Moreover, from the calculated (not shown) local density of states for the Al atom close to the surface and its nearest C atoms atom Al is evident a strong coupling between Al-p states and C-sp^2 hybrids of the monovacancy, in agreement with other periodic DFT calculations for Al_{13} adsorbed on defective graphene [8]. Therefore, the addition of a second Al atom to the graphene vacancy yields a material with different electronic transport properties, compared to atomic adsorbed Al, in relation to its possible use as gas detector.

4. Conclusions

In the present work a combined cluster-plus-slab approach was used to study the adsorption of Al on a monovacancy of graphene. The discrepancy in the number of configurations obtained with different functionals and surface models indicate that several geometries are metastable states; however, all the calculations agree with the global minimum: the H3–H3 configuration with Al atoms on both sides of the monovacancy. The second more stable structure is the H3-B geometry, with both atoms on the same side of the graphene plane. Besides, the magnitude of the adsorption energy is larger than that of an individual adsorbed atom on the same defect. While the ground state for free Al_2 and the naked defective graphene is a triplet, that corresponding to Al_2 adsorbed on the monovacancy is a singlet.

Aluminum dimers behave as effective electron donors on a defective graphene. Indeed, a significant electron transfer from Al to the sheet is produced, of about 2*e* for the more stable adsorption geometries. Furthermore, the graphene surface acts enhancing the Al–Al bond.

The Al_2/defective graphene system with a doping of about 3% for H3 and H3-B geometries has a nearly zero band gap with almost no states at the Fermi level, at difference with the situation where only one adsorbed Al atom is adsorbed on the monovacancy which behaves as a metal. This semiconductor behavior, together with the high stability of the adsorbed dimer, makes this system as a good candidate for its potential use as gas sensors.

Acknowledgements

The authors want to acknowledge the financial support of these Argentine institutions: Consejo Nacional de Investigaciones Científicas y Técnicas, Agencia Nacional de Promoción Científica y Tecnológica and Universidad Nacional del Sur, under Grants PIP N°112-200801-02286, PICT-2010-0830 and PGI 24/F05, respectively.

References

[1] O. Leenaerts, P. Partoes, F.M. Peeters, Adsorption of H_2O, NH_3, CO, NO_2 and NO on graphene: a first-principle study, Phys. Rev. B 77 (2008) 125416 (6 pp).
[2] Y.-H. Zhang, Y.-B. Chen, K.-G. Zhou, C.-H. Liu, J. Zeng, H.-L. Zhang, Y. Peng, Improving gas sensing properties of graphene by introducing dopants and defects: a first-principles study, Nanotechnology 20 (2009) 185504 (8 pp).
[3] A. Hashimoto, K. Suenaga, A. Gloter, K. Urita, S. Iijima, Direct evidence for atomic defects in graphene layers, Nature 430 (2004) 870–873.
[4] Q. Ma, A. Rosenberg, Interaction of Al clusters with the (0001) surface of highly oriented pyrolitic graphite, Surf. Sci. 391 (1997) L1224–L1229.
[5] K.T. Chan, J.B. Neaton, M.L. Cohen, First-principles study of metal adatom adsorption on graphene, Phys. Rev. B 77 (2008) 235430 (12 pp).
[6] N.F. Domancich, R.M. Ferullo, N.J. Castellani, DFT study on the interaction between atomic aluminum and graphene, J. Theor. Comput. Chem. 13 (7) (2014) 1450055 (18 pp).
[7] I. Moullet, Ab-initio molecular dynamics study of the interaction of aluminium clusters on a graphite surface, Surf. Sci. 331–333 (1995) 697–702.
[8] D.-H. Lim, A. Suarez Negreira, J. Wilcox, DFT studies on the interaction of defective graphene-supported Fe and Al nanoparticles, J. Phys. Chem. C 115 (2011) 8961–8970.
[9] O.V. Yazyev, L. Helm, Defect-induced magnetism in graphene, Phys. Rev. B 75 (2007) 125408 (5pp).
[10] R. Singh, P. Kroll, Magnetism in graphene due to single-atom defects: dependence on the concentration and packing geometry of defects, J. Phys.: Condens. Matter 21 (2009) 196002 (7 pp).
[11] P.A. Denis, Band gap opening of monolayer and bilayer graphene doped with aluminium, silicon, phosphorous, and sulfur, Chem. Phys. Lett. 492 (2010) 251–257.
[12] X. He, Z.X. Chen, Z. Li, Z. Zou, Communication: emergence of localized magnetic moment at adsorbed beryllium dimer on graphene, J. Chem. Phys. 133 (2010) 231104 (4 pp).
[13] Z. Fu, G.W. Lemire, G.A. Bishea, M.D. Morse, Spectroscopy and electronic structure of jetcooled Al_2, J. Chem. Phys. 93 (1990) 8420–8441.
[14] M.J. Frisch, et al., Gaussian 03, Revision C.02, Gaussian Inc., Wallingford, CT, 2004.
[15] R.M. Ferullo, N.F. Domancich, N.J. Castellani, On the performance of van der Waals corrected-density functional theory in describing the atomic hydrogen physisorption on graphite, Chem. Phys. Lett. 500 (2010) 283–286.
[16] Y. Ferro, A. Allouche, F. Marinelli, C. Brosset, Theoretical study of oxygen adsorption on boron-doped graphite, Surf. Sci. 559 (2004) 158–168.
[17] N. Rougeau, D. Teillet-Billy, V. Sidis, Double H atom adsorption on a cluster model of a graphite surface, Chem. Phys. Lett. 431 (2006) 135–138.
[18] M. Bonfanti, R. Martinazzo, G. Tantardini, A. Ponti, Physisorption and diffusion of hydrogen atoms on graphite from correlated calculations on the H-coronene model system, J. Phys. Chem. C 111 (2007) 5825–5829.
[19] Y. Su, X. Gao, J. Zhao, Reaction mechanisms of graphene oxide chemical reduction by sulfur-containing compounds, Carbon 67 (2014) 146–155.
[20] H. Tachikawa, T. Iyama, H. Kawabata, Effect of hydrogenation on the band gap of graphene nano-flakes, Thin Solid Films 554 (2014) 199–203.
[21] J.P. Perdew, K. Burke, M. Ernzerhof, Generalized gradient approximation made simple, Phys. Rev. Lett. 77 (1996) 3865–3868.
[22] A.D. Becke, Density-functional thermochemistry. III. The role of exact exchange, J. Chem. Phys. 98 (1993) 5648–5652.
[23] A.E. Reed, L.A. Curtiss, F. Weinhold, Intermolecular interactions from a natural bond orbital, donor–acceptor viewpoint, Chem. Rev. 88 (1988) 899–926.
[24] G. Kresse, J. Furthmüller, Efficient iterative schemes for *ab initio* total-energy calculations using a plane-wave basis set, Phys. Rev. B 54 (1996) 11169–11186.
[25] G. Kresse, J. Furthmüller, Efficiency of ab-initio total energy calculations for metals and semiconductors using a plane-wave basis set, Comput. Mater. Sci. 6 (1996) 15–50.
[26] P. Blöchl, Projector augmented-wave method, Phys. Rev. B 50 (1994) 17953–17979.
[27] G. Kresse, D. Joubert, From ultrasoft pseudopotentials to the projector augmented-wave method, Phys. Rev. B 59 (1999) 1758–1775.
[28] H.J. Monkhorst, J.D. Pack, Special points for Brillouin-zone integrations, Phys. Rev. B 13 (1976) 5188–5192.
[29] T.H. Upton, Low-lying valence electronic states of the aluminum dimer, J. Phys. Chem. 90 (1986) 754–759.
[30] C.W. Bauschlicher Jr., H. Partridge, S.R. Langhoff, P.R. Taylor, S.P. Walch, Accurate ab-initio calculations which demonstrate a $3\Pi_u$ ground state for Al_2, J. Chem. Phys. 86 (1987) 7007–7012.
[31] D.E. Woon, T.H. Dunning Jr., Benchmark calculations with correlated molecular wave functions. VI. Second row A2 and first row/second row diatomic molecules, J. Chem. Phys. 101 (1994) 8877–8893.
[32] N. Drebov, R. Ahlrichs, Small clusters of aluminum and tin: highly correlated calculations and validation of density functional procedures, J. Chem. Phys. 134 (2011) 124308 (8 pp).
[33] P.A. Denis, When noncovalent interactions are stronger than covalent bonds: bilayer greaphene doped with second row atoms, aluminum, silicon, phosphorus and sulfur, Chem. Phys. Lett. 508 (2011) 95–101.
[34] I. Fampiou, A. Ramasubramaniam, Binding of Pt nanoclusters to point defects in graphene: adsorption, morphology and electronic structure, J. Phys. Chem. C 116 (2012) 6543–6555.
[35] M.K. Srivastava, Y. Wang, A.F. Kemper, H.-P. Cheng, Density functional study of gold and iron clusters on perfect and defected graphene, Phys. Rev. B 85 (2012) 165444 (15 pp).